Design and Dynamic Performance Research of MR Hydropneumatic Spring Based on Multi-physics Coupling Model

Min Jiang
Nanjing University of Science and Technology
Xiaoting Rui (ruixt@163.net)
Nanjing University of Science and Technology https://orcid.org/0000-0002-6114-7685
Fufeng Yang
Nanjing University of Science and Technology
Wei Zhu
Nanjing University of Science and Technology
Hongtao Zhu
Nanjing University of Science and Technology
Wenjiao Han
Nanjing University of Science and Technology

Research Article

Keywords: Magnetorheological(MR), Hydro-pneumatic spring, structural design, Multi-physical coupling, Nonlinear modeling

Posted Date: August 10th, 2022

DOI: https://doi.org/10.21203/rs.3.rs-1852410/v1

Design and Dynamic Performance Research of MR Hydro-pneumatic Spring Based on Multi-physics Coupling Model

Min Jiang, Xiaoting Rui*, Fufeng Yang, Wei Zhu, Hongtao Zhu, Wenjiao Han
(Institute of Launch Dynamics, Nanjing University of Science and Technology, Nanjing, P. R. China)

Abstract: Aiming at the problem that the damping coefficient of the traditional hydro-pneumatic spring cannot be adjusted in real-time, the magnetorheological (MR) damping technology was introduced into the traditional hydro-pneumatic spring with single gas chamber. A new shear-valve mode MR hydro-pneumatic spring was proposed. And its dynamic performance was analyzed based on multi-physical coupling simulation and mechanical property test. Firstly, a structural scheme of MR hydro-pneumatic suspension was proposed to ensure the original height adjustment function based on the working principle of traditional hydro-pneumatic suspension with single gas chamber. Secondly, based on the design requirements, the parameter of MR hydro-pneumatic spring damping structure was designed by using MR damper design method. Thirdly, the multi-physical coupling dynamic performance of the MR hydro-pneumatic spring damping structure was analyzed based on the electromagnetic field analysis theory, flow field analysis theory and thermal field analysis theory. The analysis results showed that the designed MR hydro-pneumatic spring has reasonable magnetic circuit structure and excellent working performance. Then, the mechanical properties of MR hydro-pneumatic spring were tested. The results showed that the maximum damping force can reach 20kN, and the dynamic adjustable multiple can reach 6.4 times. It has good controllability and meets the design requirements. Finally, a nonlinear model of MR hydro-pneumatic spring was established based on the elastic force calculation model of the gas and the Bouc-Wen model. The simulation results of the established model agree well with the experimental results, which can accurately describe the dynamic properties of the hydro-pneumatic spring. The proposed design and modeling method of the MR hydro-pneumatic spring can provide a theoretical basis for the related vibration damping devices.

Keywords: Magnetorheological(MR); Hydro-pneumatic spring; structural design; Multi-physical coupling; Nonlinear modeling

1. Introduction

Hydro-pneumatic suspension is one of the main types of vehicle suspension. It uses compressed gas (such as high-pressure nitrogen) as the elastic medium and hydraulic oil as the force transmission and damping medium. It has good nonlinear stiffness and damping characteristics, and can effectively improve the ride comfort and trafficability of vehicles. It is widely used in armored vehicles, engineering machinery, mining trucks and other heavy vehicles [1-4]. After decades of development and improvement, the hydro-pneumatic suspension has many structural forms. According to the number and form of accumulators, it can be divided into hydro-pneumatic

* *Corresponding author: Institute of Launch Dynamics, Nanjing University of Science and Technology, 200 Xiaolingwei, Nanjing, P. R. China.*
Email: ruixt@163.net

suspension with single gas chamber, hydro-pneumatic suspension with double gas chamber and two-stage partial pressure hydro-pneumatic suspension [5-7]. According to whether the suspension actuating cylinder is connected, it can be divided into independent hydro-pneumatic suspension and connected hydro-pneumatic suspension. According to different control modes, it can be divided into passive hydro-pneumatic suspension, semi-active hydro-pneumatic suspension [8] and active hydro-pneumatic suspension [9]. At present, there are many types of hydro-pneumatic suspension, and each type has corresponding performance advantages. When applied, the corresponding type can be selected according to the actual work requirements.

As the core component of hydro-pneumatic suspension, hydro-pneumatic spring provides stiffness and damping for the suspension system. At present, the hydro-pneumatic spring mainly adopts two damping structures: fixed gap valve type and adjustable valve type. The corresponding hydro-pneumatic suspension types of the two are passive and active respectively. Passive hydro-pneumatic suspension cannot reduce vibration in real time according to road conditions and vehicle driving state. And it is difficult to maintain the best ride comfort during driving. Active hydro-pneumatic suspension has many disadvantages, such as complex structure, cost high, high energy consumption, difficult maintenance. And because the hydro-pneumatic spring is the bearing part of suspension system. It breaks down when the vehicle is running, which will lead to a major accident. Therefore, the active hydro-pneumatic suspension is still in the experimental stage and has not been applied. With the rapid development of MR technology, MR dampers, which have the advantages of simple structure, large output, low energy consumption, fast response, failure safety, have been widely applied in vehicle suspension [10-12]. This makes it possible to introduce MR semi-active damping technology into hydro-pneumatic suspension to develop a new MR semi-active hydro-pneumatic suspension and improve vehicle ride comfort.

As the core component of MR semi-active suspension, the working performance of MR damper will directly determine the vibration reduction performance of suspension. The working principle of MR damper is to change the rheological properties of the MR fluid by adjusting it's working magnetic field intensity, so as to realize the purpose of adjustable damping force. Because MR fluid is a non-Newtonian fluid whose rheological properties change with the magnetic field intensity. Therefore, the working performance of MR damper is determined by the mutual coupling of internal structure, MR fluid and electromagnetic field. In the design, the coupling analysis of multiple-physical fields is needed to consider the influence of working magnetic field and flow state of MR fluid on its dynamic performance. Parlak et al. [13] proposed an optimization design method for magnetic fluid coupling simulation of MR dampers by finite element simulation software ANSYS and CFX. The distribution of flow field under the action of magnetic field in the damper was obtained. However, the simulation steps are complex, the amount of calculation is large, and the influence of uneven magnetic field distribution in the damper is not considered. Goldasz et al. [14] established the simulation model of the squeeze MR damper based on the apparent viscosity method. The relationship between the damping force and the loading frequency was obtained. And the relationship between the damping force and the

current was obtained. However, this method is only based on theoretical modeling and does not involve finite element analysis. The distribution law of magnetic field and flow field inside the damper cannot be obtained. Wael et al. [15] proposed a novel one-way coupled numerical approach for dynamic performance analysis of the MR damper based on electromagnetic field finite element analysis method and fluid dynamics analysis method. Taking MR fluid as incompressible one-way flow and two-phase flow respectively, the distribution of fluid pressure, velocity and viscosity in MR damper was simulated and analyzed. The simulation results showed that the fluid compressibility has a great influence on the hysteresis characteristics of MR damper. Mario et al. [16] made a static analysis of the internal electromagnetic field and thermal field of the MR damper by the finite element software ANSYS. The analysis results showed that temperature not only affects the viscosity of the liquid, but also affects the magnetization process of magnetic materials. With the increase of temperature, the viscosity of liquid decreases, and the saturation magnetic field intensity of magnetic materials decreases. To sum up, the working performance of MR damper is determined by the internal structure and multiple physical fields at the same time. So it is necessary to analyze the dynamic performance of multiple physical fields coupling during structural design to ensure that the structural design is reasonable and the performance meets the design requirements. At present, the multi-physical field analysis methods include numerical method and finite element software [17, 18]. The finite element software does not need engineers to deduce the multi-physical field coupling equation of the system, and the solution process is simple. It is favored by a large number of scholars. Therefore, the finite element software Comsol is used to analyze the dynamic performance of MR hydro-pneumatic spring in this paper.

Aiming at the shortcomings of the existing hydro-pneumatic suspension products that can not realize continuous adjustment of damping and have poor adaptability to different driving conditions and road excitation, the MR technology was introduced into hydro-pneumatic suspension, and a MR hydro-pneumatic spring with adaptive damping function was proposed in this paper. The multi-physical coupling dynamic performance of the MR hydro-pneumatic spring damping structure was analyzed based on the electromagnetic field analysis theory, flow field analysis theory and thermal field analysis theory. The structure design and dynamic performance analysis of MR hydro-pneumatic suspension were completed based on multi- physics coupling simulation and mechanical performance test. Following were the main contents. Firstly, the structural scheme and working principle of the MR hydro-pneumatic suspension were described. Secondly, the main parameters of the MR hydro-pneumatic spring damping structure were designed. Thirdly, the multi-physical coupling dynamic performance of the MR hydro-pneumatic spring damping structure was analyzed. Fourthly, the mechanical properties of the MR hydro-pneumatic spring were tested and the dynamic characteristics were analyzed. The nonlinear model of the MR hydro-pneumatic spring was established based on the test results. Finally, the research content of this paper was summarized.

2. Structural scheme of MR hydro-pneumatic suspension

The hydraulic principle diagram of the traditional hydro-pneumatic suspension system with single gas chamber is shown in Figure 1. It is mainly composed of hydraulic cylinder, piston, damping valve group, accumulator (filled with high-pressure nitrogen), height adjustment valve group, safety valve group, oil pump and oil tank. The piston, hydraulic cylinder, damping valve group and accumulator form a hydro-pneumatic spring with single gas chamber, which is used as the elastic element and damping element of hydro-pneumatic suspension. The height adjustment valve group is mainly used to fill or drain the hydraulic cylinder through the oil pump to realize the height adjustment of the vehicle body. When the compression stroke, the piston moves upward relative to the hydraulic cylinder. The piston compresses the hydraulic oil in the upper chamber of the hydraulic cylinder. The compression valve is opened. The hydraulic oil in the upper chamber of the hydraulic cylinder is forced into the accumulator. The gas in the accumulator is compressed. When in the extension stroke, the piston moves downward relative to the hydraulic cylinder. The pressure in the upper chamber of the hydraulic cylinder decreases. The gas in the accumulator expands. The extension valve is opened. The hydraulic oil in the accumulator is forced into the upper chamber of the hydraulic cylinder. When the vehicle is stationary, the height adjustment of the vehicle body can be realized through the height adjustment valve group in the hydro-pneumatic suspension. When the lift valve works, the hydraulic oil is charged into the hydro-pneumatic spring through the oil pump. The piston moves downward relative to the hydraulic cylinder to raise the body. When the lowering valve works, the hydraulic oil in the hydro-pneumatic spring flows into the oil tank through the lowering valve. The piston moves upward relative to the hydraulic cylinder, and the hydro-pneumatic spring is compressed. The body height is reduced.

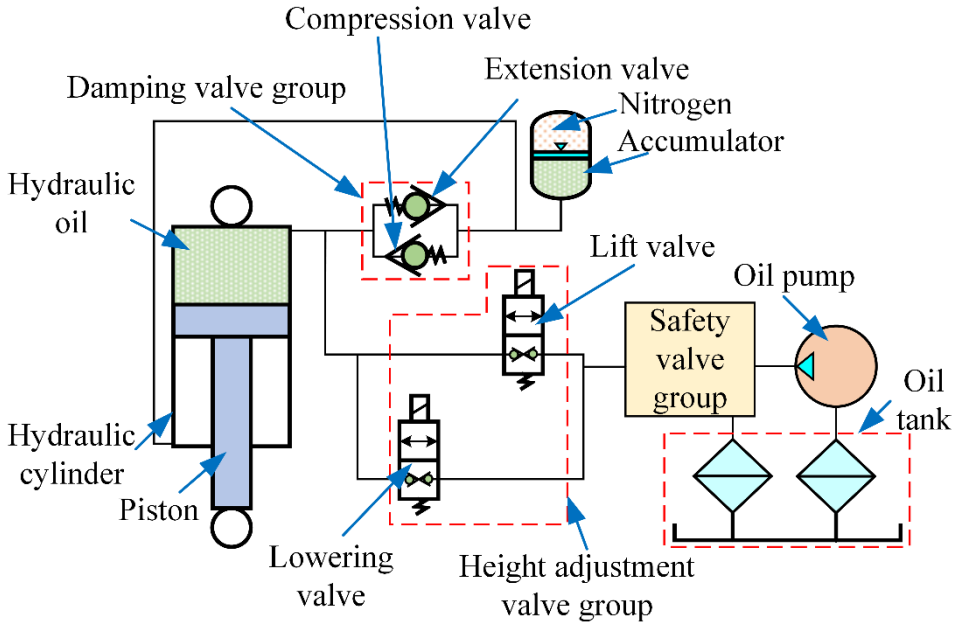

Figure 1. Hydraulic principle diagram of the traditional hydro-pneumatic suspension system

It can be seen from the above introduction that the performance parameters (damping, stiffness, etc.) of the traditional hydro-pneumatic suspension system cannot change with the road conditions and driving state. It belongs to the passive hydro-pneumatic suspension system, which is difficult to realize that the vehicle has good ride comfort, operational stability and other working performance under different working conditions. In order to ensure that the vehicle has the best damping state in different driving conditions, this paper introduces the MR damping technology into the hydro-pneumatic suspension system to realize the real-time adjustable damping. On the basis of ensuring the height adjustment function of the original passive hydro-pneumatic suspension system, the MR hydro-pneumatic suspension system is designed. The hydraulic principle diagram of the designed MR hydro-pneumatic suspension system is shown in Figure 2.

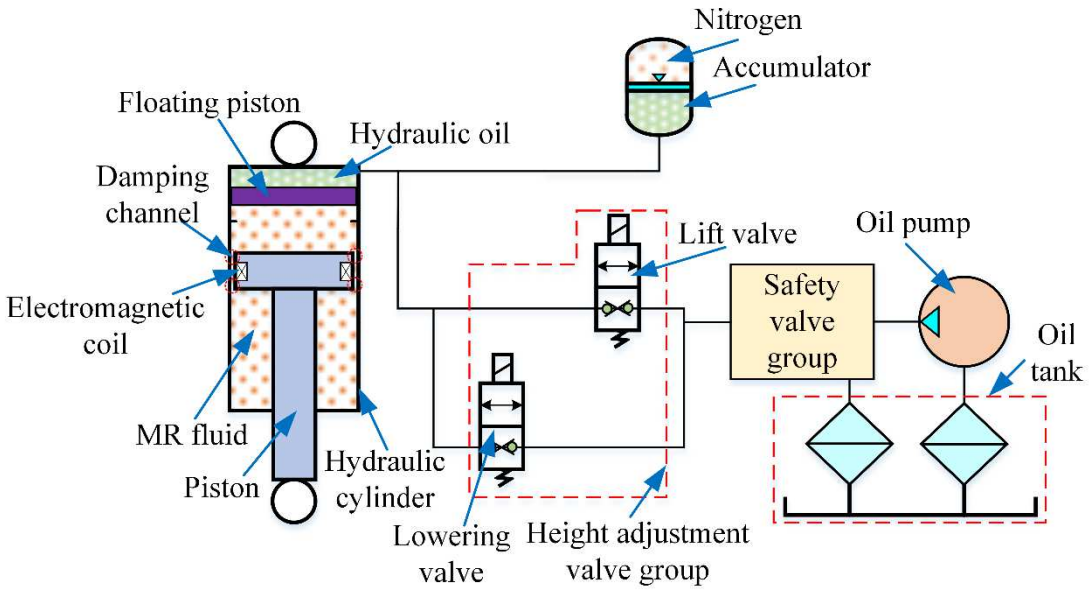

Figure 2. Hydraulic principle diagram of the MR hydro-pneumatic suspension system

The main difference between the MR hydro-pneumatic suspension and the passive hydro-pneumatic suspension is that the MR fluid damper is introduced into the hydro-pneumatic spring. The damping valve group is removed. And other structures are basically unchanged. The MR hydro-pneumatic spring is mainly composed of piston, hydraulic cylinder, MR fluid, electromagnetic coil, floating piston, hydraulic oil and accumulator. The outer surface of the piston and the inner surface of the hydraulic cylinder form a MR fluid working gap, that is, a damping channel. The floating piston divides the working cylinder into two chambers, namely, hydraulic oil chamber and MR fluid chamber.

When the MR hydro-pneumatic suspension is in the compression stroke, the MR fluid enters the lower chamber through the damping channel and pushes the floating piston upward. Hydraulic oil is forced into the accumulator. The gas in the accumulator is compressed. When the MR hydro-pneumatic suspension is in the extension stroke, the piston moves downward. The lower chamber MR fluid is forced to flow into the upper chamber through the damping channel. At the same time, the gas expansion in the accumulator, forces the hydraulic oil into the hydraulic oil chamber. The hydraulic

oil pushes the floating piston downward. During the compression and extension stroke, the magnetic field strength in the damping channel can be adjusted by adjusting the working current of the electromagnetic coil. And then the damping force can be adjusted to realize continuous and adjustable damping.

3. Structural design of MR hydro-pneumatic spring

According to the structural scheme of MR hydro-pneumatic spring, its structure can be divided into three parts: MR damping structure, force transmission structure and elastic structure. Because the MR hydro-pneumatic suspension designed in this paper needs to ensure the basic functions of the passive hydro-pneumatic suspension system. And its force transmission structure and elastic structure are basically unchanged. This paper mainly designs the MR damping structure with continuous adjustment of damping when designing the MR hydro-pneumatic spring.

The shear-valve mode MR damper is used in the MR damping structure. It controls the magnetic field strength of the damping channel by controlling the working current of the electromagnetic coil, so as to realize the continuous adjustment of the damping force. According to the damping force calculation model and working principle of the MR damper, the main parameters that need to be designed for the MR damping structure include the inner diameter of the cylinder D_{5y}, the outer diameter of the cylinder D_{4y}, the diameter of the piston rod d_y, the diameter of the piston D_y, the diameter of the iron core D_{3y}, the length of the iron core L_{1y}, the damping gap h_y and the length damping channel L_y, as shown in Figure 3.

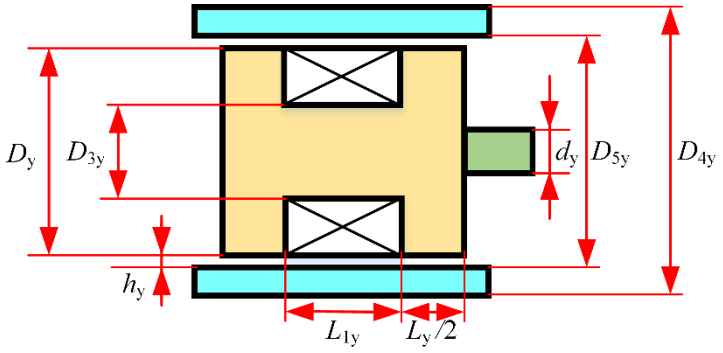

Figure 3. Structural parameters of the MR damping structure

3.1 Design requirements

According to the design requirements of the hydro-pneumatic suspension system of an armored vehicle, the design requirements of the MR hydro-pneumatic spring damping structure are shown in Equation (1).

$$\begin{cases} F_{dy} \geq 15000\text{N} \quad v_y = 0.12\text{m/s} \\ \beta_{dy} \geq 5 \\ s_y = 260\text{mm} \end{cases} \tag{1}$$

Where, F_{dy} denotes the damping force of the MR hydro-pneumatic spring; v_y denotes the relative velocities of piston and master cylinder; β_{dy} denotes the damping adjustable coefficient of the MR hydro-pneumatic spring; s_y indicates the stroke of

MR hydro-pneumatic spring.

3.2 Structural design

The working mode of the MR hydro-pneumatic spring damping structure is the shear-valve mode. According to the flow field analysis of the MR damper, the calculation model of the damping force of the shear-valve MR damper can be applied to the calculation model of the valve MR damper, as shown in Equation (2) [19].

$$F_{\mathrm{dy}}=\frac{12\mu_{\rho}L_{\mathrm{y}}A_{\mathrm{py}}^{2}}{\pi D_{\mathrm{y}}h_{\mathrm{y}}^{3}}v_{\mathrm{y}}+\frac{3L_{\mathrm{y}}A_{\mathrm{py}}\tau_{\mathrm{y}}}{h_{\mathrm{y}}}\mathrm{sgn}(v_{\mathrm{y}})=F_{\eta\mathrm{y}}+F_{\tau\mathrm{y}} \tag{2}$$

Where, $F_{\eta\mathrm{y}}$ is the viscous damping force; $F_{\tau\mathrm{y}}$ is coulomb damping force; $A_{\mathrm{py}}=[\pi(D_{\mathrm{y}}^{2}-d_{\mathrm{y}}^{2})]/4$ is the effective area of the piston; μ_{ρ} is plastic viscosity; τ_{y} is the yield stress of MR fluid.

The magnetic circuit is made of low carbon steel with carbon content of 0.2%. Its magnetic characteristics are shown in Table 1. And BH curve is shown in Figure 4.

Table 1. Magnetic properties of low carbon steel

Initial permeability μ_{i}	Maximum permeability $\mu_{\max}$	Saturation magnetic induction $B_{\mathrm{s}}(T)$	Coercive force H_{c}(A/m)	Resistivity $P(\Omega\cdot\mathrm{cm})$
553	1580	1.50	147	1.81×10^{-6}

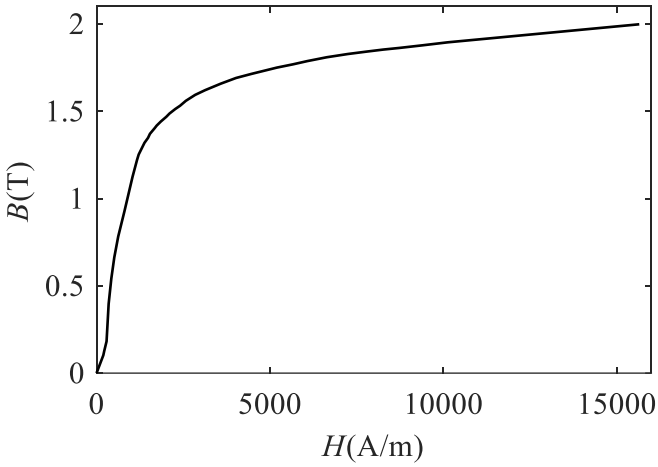

Figure 4. BH curve of carbon steel with carbon content of 0.2%

MRF-J25 produced by Chongqing Materials Research Institute is selected as MR fluid of the designed MR damper. Its physical characteristics are shown in Table 2. And BH curve is shown in Figure 5. According to literature [20], the flow characteristics of MR fluid can be simulated by Bingham-Papanasasiou model, as shown in Equation (3).

Table 2. Physical properties of MRF-J25T

Characteristic	Value
Viscosity（Pa·s）	0.8
Density（$\mathrm{g\cdot cm^{-3}}$）	2.65
Magnetization property M_{s} (kA/m)	379.64
Operating temperature（℃）	-40~130

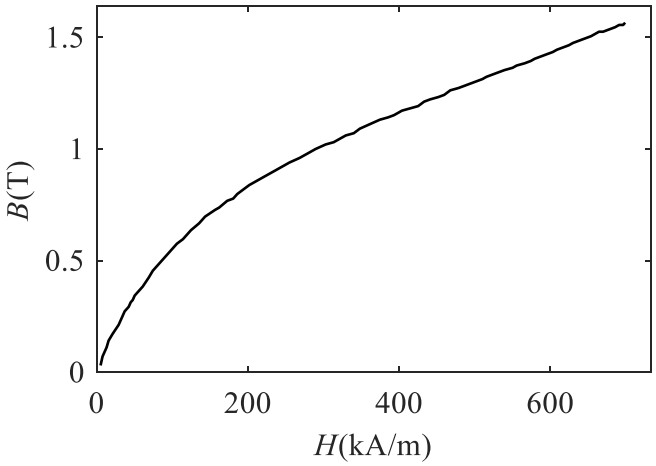

Figure 5. BH curve of MRF-J25 BH

$$\begin{cases} \tau=\mu_{\rho}\dot{\gamma}+\tau_{y}(1-e^{-m_{\rho}\dot{\gamma}}) \\ \tau_{y}=-24520B^{3}+58920B^{2}+11250B \\ m_{\rho}=0.02536B^{2}-0.0533B+0.03453 \end{cases} \tag{3}$$

Where, τ denotes shear stress; $\dot{\gamma}$ denotes shear rate; m_{ρ} denotes model parameter.

Based on the design method in my previous research on MR damper design [19], main structural parameters of MR hydro-pneumatic spring damping structure are designed, as shown in Table 3.

Table 3. Main structural parameters of MR damping structure

Parameters	Values	Parameters	Values
D_{y}	137.00mm	D_{4y}	158.00mm
L_{y}	34.00mm	D_{5y}	140.00mm
h_{y}	1.50mm	d_{y}	90.00mm
D_{3y}	72.00mm	L_{1y}	30.00mm

In order to ensure the reliability of damping force, in the actual calculation process, the critical shear stress of MR fluid is taken as 20kPa. Substitute the above parameters into Equation (2) to calculate the maximum damping force.

$$F_{\eta y}=\frac{12\eta_{\mathrm{MRF}}L_{y}A_{py}^{2}}{\pi D_{y}h_{y}^{3}}v_{y}=1893\mathrm{N} \tag{4}$$

$$F_{\tau y}=\frac{3L_{y}A_{py}\tau_{y}}{h_{y}}=14245\mathrm{N} \tag{5}$$

$$F_{dy}=F_{\eta y}+F_{\tau y}=16138\mathrm{N} \tag{6}$$

The damping adjustable coefficient can be obtained from Equation (4) and Equation (5), such as Equation (7).

$$\beta_{\mathrm{dy}}=\frac{F_{\tau \mathrm{y}}}{F_{\eta \mathrm{y}}}=7.5 \tag{7}$$

From Equation (6) and Equation (7), it can be seen that the designed MR hydro-pneumatic spring meets the design requirements.

4. Multi-physical analysis of MR hydro-pneumatic spring

The main working principle of MR hydro-pneumatic spring is to change the rheological characteristics of MR fluid by adjusting the working magnetic field strength, so as to achieve the purpose of adjustable damping force. Because MR fluid is a non-Newtonian fluid. The working characteristics of the MR hydro-pneumatic spring, the distribution of electromagnetic field in damping channel and the state of MR fluid are affected by multiple-physical fields. In order to more accurately explore the overall performance of the MR hydro-pneumatic spring under the action of multiple-physical fields. The finite element software Comsol is used to analyze the dynamic performance of the designed MR hydro-pneumatic spring in the electric-magnetic-fluid-solid-thermal multi-physical fields. The simulation flow chart is shown in Figure 6.

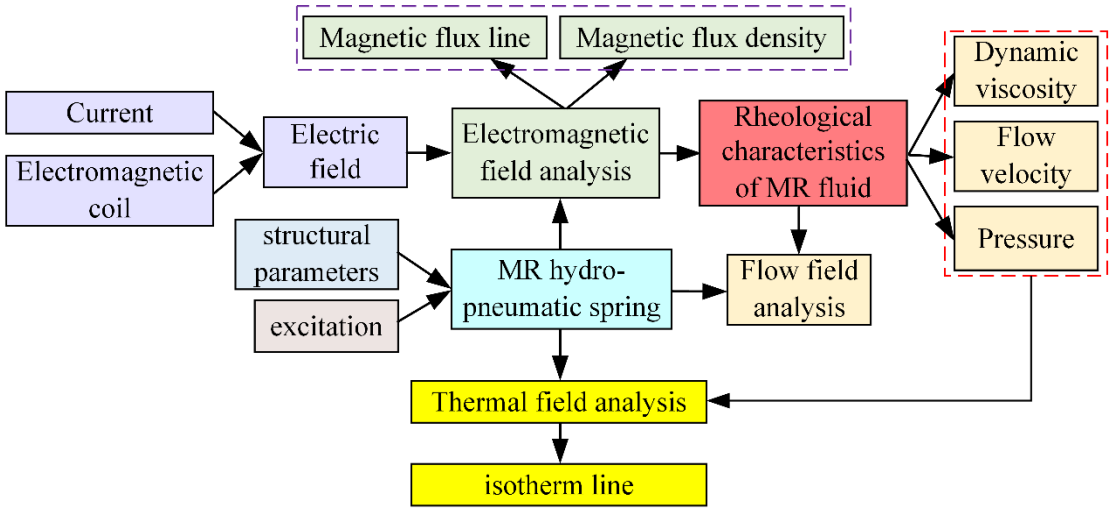

Figure 6. The flow chart of the multi-physical analysis

4.1 Electromagnetic field analysis model

The static electromagnetic field distribution of the magnetic circuit can be solved by Maxwell equations [21]. According to ampere loop law, the magnetic field intensity vector $\boldsymbol{H}$ can be solved by Equation (8).

$$\nabla \times \boldsymbol{H}=\boldsymbol{J} \tag{8}$$

Where, ∇ is Hamiltonian operator; $\boldsymbol{J}$ is the current density vector, and the mathematical expression is shown in Equation (9).

$$\boldsymbol{J}=\sigma \boldsymbol{v} \times \boldsymbol{B}+\boldsymbol{J}_{\mathrm{e}} \tag{9}$$

Where, $\boldsymbol{B}$ is the magnetic flux density vector; $\boldsymbol{J}_{\mathrm{e}}$ is the external current density; $\boldsymbol{v}$ is the velocity of the conductor.

The relationship between magnetic flux density vector $\boldsymbol{B}_{\mathrm{r}}$ and magnetic field intensity vector $\boldsymbol{H}_{\mathrm{r}}$ of linear magnetic conducting material is shown in Equation (10).

$$\boldsymbol{B}_{\mathrm{r}}=\mu_0\mu_{\mathrm{r}}\boldsymbol{H}_{\mathrm{r}} \tag{10}$$

Where, μ_0 is vacuum permeability; μ_{r} is the relative permeability of the magnetic circuit.

The relationship between magnetic flux density vector $\boldsymbol{B}_{\mathrm{r}}$ and magnetic field intensity vector $\boldsymbol{H}_{\mathrm{r}}$ of nonlinear soft magnetic materials can be determined by BH curve, as shown in Equation (11).

$$\boldsymbol{B}_{\mathrm{n}}=f(|\boldsymbol{H}_{\mathrm{n}}|) \tag{11}$$

Where, $f(\ )$ is the function symbol.

The current excitation of the electromagnetic field in the magnetic circuit is only provided by the electromagnetic coil. The weak eddy current phenomenon generated when the excitation coil reciprocates with the piston head is ignored, that is, $\sigma\boldsymbol{v}\times\boldsymbol{B}=0$. $\boldsymbol{J}$ can be obtained from Equation (6), as shown in Equation (12).

$$\boldsymbol{J}=\boldsymbol{J}_{\mathrm{e}}=\frac{NI}{S_{\mathrm{coil}}}\boldsymbol{e}_{\mathrm{n}} \tag{12}$$

Where, N is the number of turns of the electromagnetic coil; I represents the working current of electromagnetic coil; S_{coil} is the sectional area of the electromagnetic coil; $\boldsymbol{e}_{\mathrm{n}}$ is the unit vector of the direction of positive charge movement.

The electromagnetic field analysis model of the magnetic circuit can be obtained from Equation (8), Equation (10), Equation (11) and Equation (12), as shown in Equation (13).

$$\begin{cases}\nabla\times\boldsymbol{H}_{\mathrm{r}}=\dfrac{NI}{S_{\mathrm{coil}}}\boldsymbol{e}_{\mathrm{n}}\\ \boldsymbol{B}_{\mathrm{r}}=\mu_0\mu_{\mathrm{r}}\boldsymbol{H}_{\mathrm{r}}\\ \nabla\times\boldsymbol{H}_{\mathrm{n}}=\dfrac{NI}{S_{\mathrm{coil}}}\boldsymbol{e}_{\mathrm{n}}\\ \boldsymbol{B}_{\mathrm{n}}=f(|\boldsymbol{H}_{\mathrm{n}}|)\end{cases} \tag{13}$$

4.2 Flow field analysis model

The rheological properties of MR fluid change sharply under the action of external magnetic field, that is, MR effect. When analyzing the internal flow field of the MR hydro-pneumatic spring damping structure, MR fluid is regarded as a single-phase fluid. And it is assumed that it is an incompressible fluid not affected by temperature. The flow state of MR fluid can be described by Navier-Stokes equations [22], as shown in Equation (14).

$$\begin{cases} \rho\dfrac{\partial \boldsymbol{u}}{\partial t}+\rho(\boldsymbol{u}\cdot\nabla)\boldsymbol{u}=\nabla\cdot\left[-p\boldsymbol{E}+\mu(\nabla\boldsymbol{u}+(\nabla\boldsymbol{u})^{\mathrm{T}})\right]+\boldsymbol{F}_{\mathrm{v}} \\ \rho\nabla\cdot\boldsymbol{u}=0 \end{cases} \tag{14}$$

Where, ρ is the fluid density; $\boldsymbol{u}$ is flow velocity; $\boldsymbol{E}$ is the unit tensor; p is the pressure; μ_{p} is dynamic viscosity; $\boldsymbol{F}_{\mathrm{v}}$ is the volume force.

The flow state of MR fluid in the damping channel is determined by Reynolds number R_{e}, as shown in Equation (15).

$$R_{\mathrm{e}}=\frac{\rho|\boldsymbol{u}|h}{\mu_{\mathrm{p}}} \tag{15}$$

The value of R_{e} in the MR hydro-pneumatic spring is far less than 2300, so MR fluid is in laminar flow state.

The relationship between the rheological properties of MR fluid and magnetic field can be described by Bingham-Papanasasiou model of non-Newtonian fluid, without considering the influence of temperature and shear thinning, as shown in Equation (16).

$$\tau=\mu_{\mathrm{p}}\dot{\gamma}+\tau_{\mathrm{y}}(1-e^{-m_{\mathrm{p}}\dot{\gamma}}) \tag{16}$$

From Equation (3) and Equation (16), the mathematical expression of dynamic viscosity of MR fluid is shown in Equation (17).

$$\mu=\frac{\tau}{\dot{\gamma}}=\mu_{\mathrm{p}}+\frac{\tau_{\mathrm{y}}(B)}{\dot{\gamma}}(1-e^{-m_{\mathrm{p}}\dot{\gamma}}) \tag{17}$$

Where, $\tau_{\mathrm{y}}(B)$ represents the function of τ_{y} with respect to B.

The volume force of MR fluid in the magnetic field environment is the magnetic penetration force generated by the magnetic field, as shown in Equation (18).

$$\boldsymbol{F}_{\mathrm{v}}=\mu_0\boldsymbol{M}\cdot\nabla\times H \tag{18}$$

According to Equation (14), Equation (17) and Equation (18), the internal flow field analysis model of the MR hydro-pneumatic spring damping structure can be obtained, as shown in Equation (19).

$$\begin{cases} \rho\dfrac{\partial \boldsymbol{u}}{\partial t}+\rho(\boldsymbol{u}\cdot\nabla)\boldsymbol{u}=\nabla\cdot\left[-p\boldsymbol{E}+\mu(\nabla\boldsymbol{u}+(\nabla\boldsymbol{u})^{\mathrm{T}})\right]+\boldsymbol{F}_{\mathrm{v}} \\ \rho\nabla\cdot\boldsymbol{u}=0 \\ \mu=\dfrac{\tau}{\dot{\gamma}}=\mu_{\mathrm{p}}+\dfrac{\tau_{\mathrm{y}}(B)}{\dot{\gamma}}(1-e^{-m_{\mathrm{p}}\dot{\gamma}}) \\ \boldsymbol{F}_{\mathrm{v}}=\mu_0\boldsymbol{M}\cdot\nabla\times H \end{cases} \tag{19}$$

4.3 Thermal field analysis model

When the MR hydro-pneumatic spring works, the piston moves back and forth in the cylinder. The MR fluid is forced to flow from the high-pressure force chamber to the low-pressure force chamber through the damping channel. Under the pressure drop of the damping channel, the MR fluid generates Poiseuille pressure flow [23]. At the

same time, the dynamic viscosity of of the magnetorheological fluid changes with time and nonlinearity under the action of the magnetic field, there is also Couette viscous flow [24]. Vibration energy is dissipated under these two flow characteristics, as shown in Figure 7. When the position of the piston changes in the vibration damping structure, the MR fluid is forced to flow through the magnetic pole at a large shear rate (including Poiseuille pressure flow and Couette viscous flow). The internal chain of the damping channel is broken. The movement generates obvious heat, which is then convective and conductive along the axial and radial directions. In the radial direction, heat transfer includes: the internal radial convection and conduction heat transfer of magnetorheological fluid itself, the internal radial conduction of cylinder barrel, and the convection heat transfer of heat transfer with external air through the outer wall of buffer cylinder barrel. In the axial direction, heat transfer includes: axial convection and conduction heat transfer inside the magnetorheological fluid itself, and axial conduction inside the cylinder barrel. In this process, the convective heat transfer between the cylinder barrel and the external air can be expressed by Newton's convective cooling law, as shown in Equation (20) [25].

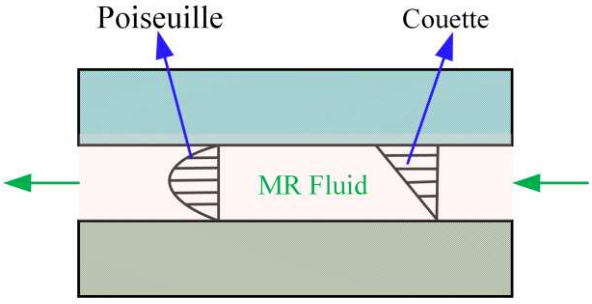

Figure 7. Flow characteristics of the MR fluid

$$\begin{cases} \Delta t = \left| t_{\text{cyl}} - t_{\text{air}} \right| \\ \Gamma = \dfrac{\Delta t}{(1/h_{\text{k}} A_{\text{k}})} \end{cases} \tag{20}$$

Where, t_{cyl} , t_{air} and Δt are the outer wall temperature, air temperature and temperature difference, respectively; $1/h_{\text{k}}A_{\text{k}}$ is the convective heat transfer resistance; Γ is the heat transfer power.

When solving the conjugate heat transfer of MR fluid and damper, heat transfer is carried out through convection and conduction in the fluid domain. And only conduction heat transfer in the solid domain. It can be assumed that there is a continuously changing temperature field between the fluid domain and the solid domain. When the damper is operated, viscous heat dissipation and pressure heat dissipation will occur. The mathematical expression of the coupled conjugate heat transfer relationship between the two is shown in Equation (21) [26]. The first and second terms on the right side of Equation (21) represent the heat source generated by pressure work and viscous heat dissipation respectively.

$$\rho C_p \frac{\partial T}{\partial t} + \rho C_p \boldsymbol{u} \cdot \nabla T + \nabla q_{\text{k}} = -\alpha_p T \frac{\partial p}{\partial t} + \mu_T [\nabla \boldsymbol{u} + (\nabla \boldsymbol{u})^{\text{T}}] \nabla \boldsymbol{u} \tag{21}$$

Where, ρ is the density of MR fluid independent of temperature and magnetic field; T is the temperature function varying with space position and time; C_p, α_p are the heat capacity (constant pressure specific heat) and thermal diffusivity under the MR fluid pressure p, respectively; q_{k} is the heat flux density of MR fluid, as shown in Equation (22); μ_T is the viscosity of MR fluid related to magnetic flux density, shear flow rate and temperature, as shown in Equation (23).

$$q_{\mathrm{k}} = h_{\mathrm{k}} \nabla t \tag{22}$$

$$\mu_T = \mu_{\rho} + \frac{\tau_{\mathrm{y}}(B)}{\dot{\gamma}}(1 - e^{-m_{\rho}\dot{\gamma}}) - \alpha(T_1 - T_0) \tag{23}$$

Where, α is the temperature coefficient; T_1 and T_0 are the temperature and initial temperature of the MR fluid at a certain time when the damper works.

From Equations (20) to (23), the thermal analysis model of the MR hydro-pneumatic spring damping structure is shown in Equation (24).

$$\begin{cases} \rho C_p \dfrac{\partial T}{\partial t} + \rho C_p \boldsymbol{u} \cdot \nabla T + \nabla q_{\mathrm{k}} = -\alpha_p T \dfrac{\partial p}{\partial t} + \mu_T [\nabla \boldsymbol{u} + (\nabla \boldsymbol{u})^{\mathrm{T}}] \nabla \boldsymbol{u} \\ \Delta t = \left| t_{\mathrm{cyl}} - t_{\mathrm{air}} \right| \\ \Gamma = \dfrac{\Delta t}{(1/h_{\mathrm{k}} A_{\mathrm{k}})} \\ q_{\mathrm{k}} = h_{\mathrm{k}} \nabla t \\ \mu_T = \mu_{\rho} + \dfrac{\tau_{\mathrm{y}}(B)}{\dot{\gamma}}(1 - e^{-m_{\rho}\dot{\gamma}}) - \alpha(T_1 - T_0) \end{cases} \tag{24}$$

4.4 Simulation analysis of multiple-physical fields

The MR hydro-pneumatic spring damping structure designed in this paper is an axisymmetric structure. In order to simplify the calculation, the 1/2 two-dimensional axisymmetric model of the damping structure can be taken as the analysis object without affecting the calculation accuracy, as shown in Figure 8. The steady electromagnetic field with different working current $I_{\mathrm{coil}} = [0, 0.2, 0.4, 0.6, 0.8, 1.0, 1.2, 1.4]\mathrm{A}$ is analyzed. Under the sinusoidal excitation with the amplitude of 20mm and the frequency of 1Hz (the piston moves relative to the cylinder), The performance of the damping structures with different working current is analyzed by multi-physical field.

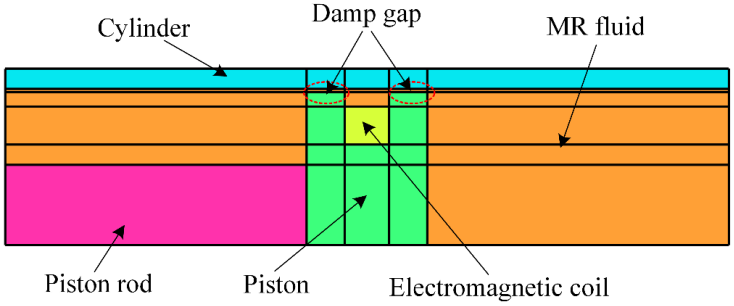

Figure 8. The 1/2 two-dimensional axisymmetric model of the damping structure

(1) Electromagnetic field simulation results

When the working current of the electromagnetic coil is 1.4A, the simulation results of the steady-state electromagnetic field of the designed magnetic circuit are shown in Figure 9, Figure 10 and Figure 12.

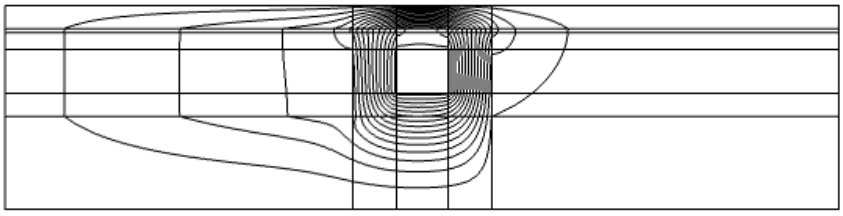

Figure 9. The distribution diagram of magnetic flux line

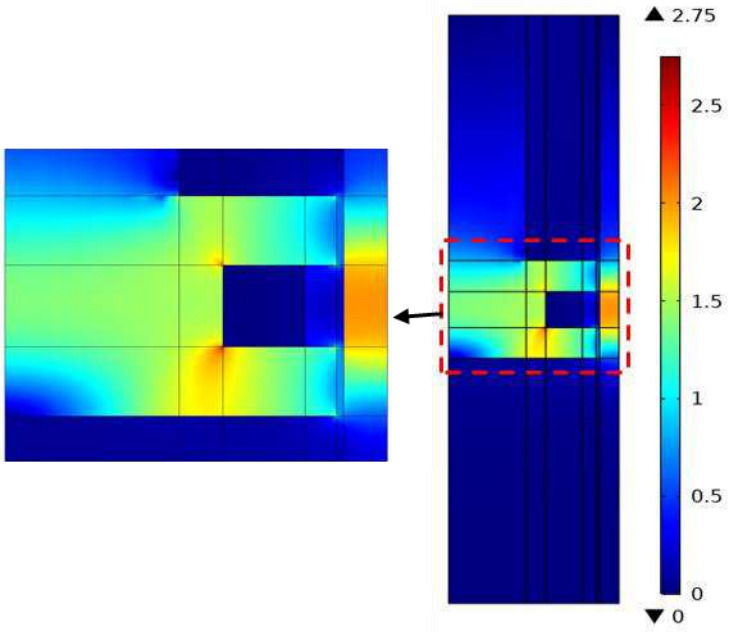

Figure 10. The distribution nephogram of magnetic flux density

When the working current of the electromagnetic coil is 1.4A, the distribution diagram of magnetic flux line of the magnetic circuit is shown in Figure 9. From the distribution of magnetic flux line, it can be seen that all the magnetic flux lines are distributed in the magnetic circuit model. The magnetic flux lines form a closed loop. And the direction of the magnetic flux line in the damping channel is perpendicular to the flow direction of the MR fluid. There is only a small amount of magnetic leakage formed by the magnetic conductivity of the piston rod. The results show that the magnetic circuit structure of the designed MR damper is reasonable. The distribution nephogram of magnetic flux density is shown in Figure 10. It can be seen from the figure that the maximum magnetic flux density is about 2T, and the magnetic flux density of iron core and working cylinder yoke is close to saturation state. The magnetic flux density in the damping channel is about 0.7T, that is, the saturated magnetic flux density when the MR fluid reaches the yield shear stress. The simulation results show that the designed magnetic circuit structure is reasonable and meets the design requirements.

The uneven distribution of magnetic field in the damping channel is considered. In order to more accurately analyze the magnetic flux density at different positions in the damping channel, an observation path is defined in the damping channel, as shown in Figure 11. The distribution of magnetic flux density in the damping channel along the path is shown in Figure 12. It can be seen from Figure 12 that the magnetic flux density in the fluid flow channel increases with the increase of the current value. And the magnetic flux density at the end of the piston yoke is the maximum value in the observation path. The magnetic flux density near the excitation coil area decreases sharply. It indicates that the piston yoke and the cylinder wall form an effective damping channel for MR fluid. The magnetic flux density at the effective damping channel increases with the increase of excitation current. When the current reaches 1.4A, the magnetic flux density slows down with the increase of current and approaches magnetic saturation.

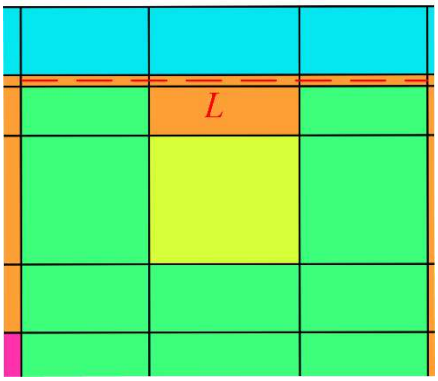

Figure 11. The observation path in the damping channel

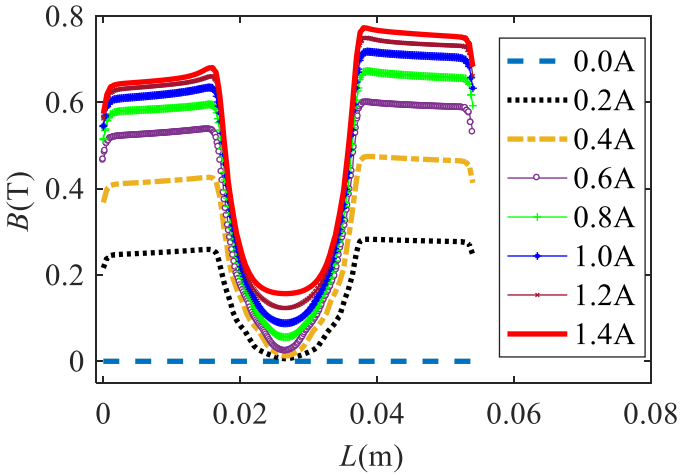

Figure 12. Distribution diagram of magnetic flux density along the observation path

(2) Magnetic flow field simulation results

Combining the electromagnetic field analysis model and the flow field analysis model, the flow state of MR fluid in the MR hydro-pneumatic spring damping structure is analyzed. The influence of temperature on the rheological effect of MR fluid is not considered in the analysis process. The simulation results are shown in Figures 13 to 17.

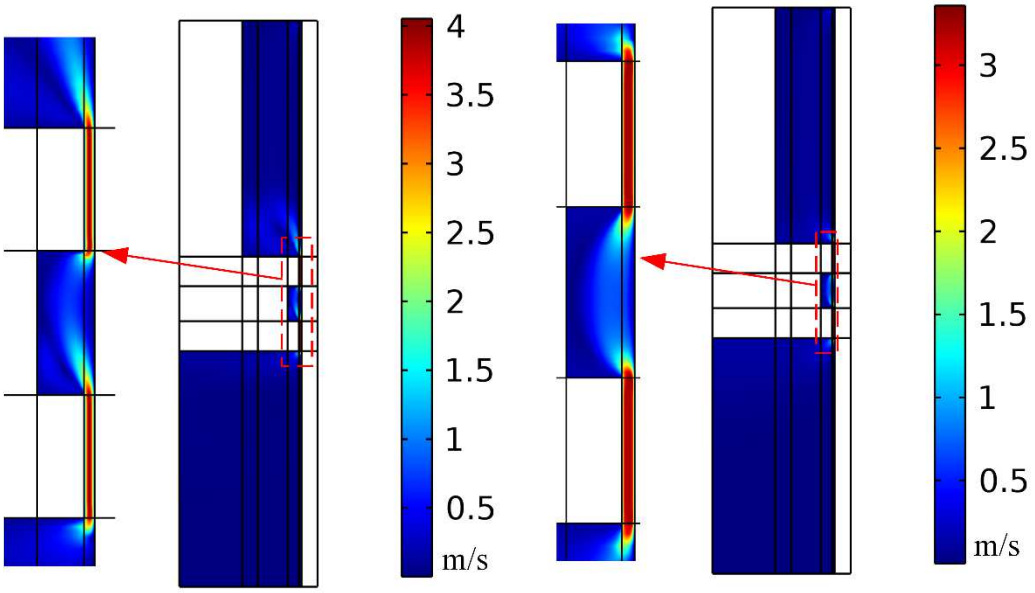

(a) 0A (b) 0.6A

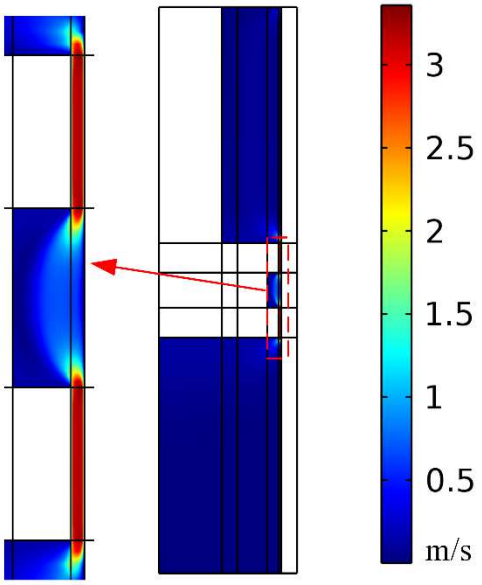

(c) 1.4A

Figure 13. The distribution nephogram of flow velocity

Under different working currents of electromagnetic coils, the flow velocity distribution nephogram and the dynamic viscosity distribution nephogram of MR fluid are shown in Figure 13 and Figure 14, respectively. It can be seen from Figure 13 that under the three working currents, the flow velocity of MR fluid in the upper and lower chambers of the cylinder is small. The flow velocity in the damping channel is large. And The flow velocity in the effective damping channel is the largest, which is mainly caused by the sharp contraction of the flow area when the MR fluid flows from the high-pressure chamber through the damping channel into the low-pressure chamber. At the same time, it can be seen that the flow velocity of MR fluid at both ends of the effective damping channel presents a jet flame distribution. It indicates that there is a large variation gradient of the flow velocity at the inlet and outlet of the effective

damping channel. It can be seen from Figure 13 (a) that when the current value is 0A, the liquid flow velocity in the effective damping channel is small on the left and right, and large in the middle. The maximum liquid flow velocity is about 4.1m/s, which is caused by the Poiseuille pressure flow caused by the pressure drop at both ends of the damping channel. It can be seen from Figure 13 (b), Figure 13 (c) and Figure 14 that after the working current is applied to the electromagnetic coil, the dynamic viscosity of MR fluid in the damping channel increases under the action of magnetic field. Poiseuille pressure flow and Couette viscous flow are generated at the same time, causing the flow velocity to decrease. It can be seen from Figure 14 that the dynamic viscosity of MR fluid increases with the increase of current value. It indicates that MR fluid produces MR effect under the action of magnetic field. And with the increase of magnetic field strength, the fluidity decreases and the yield stress increases.

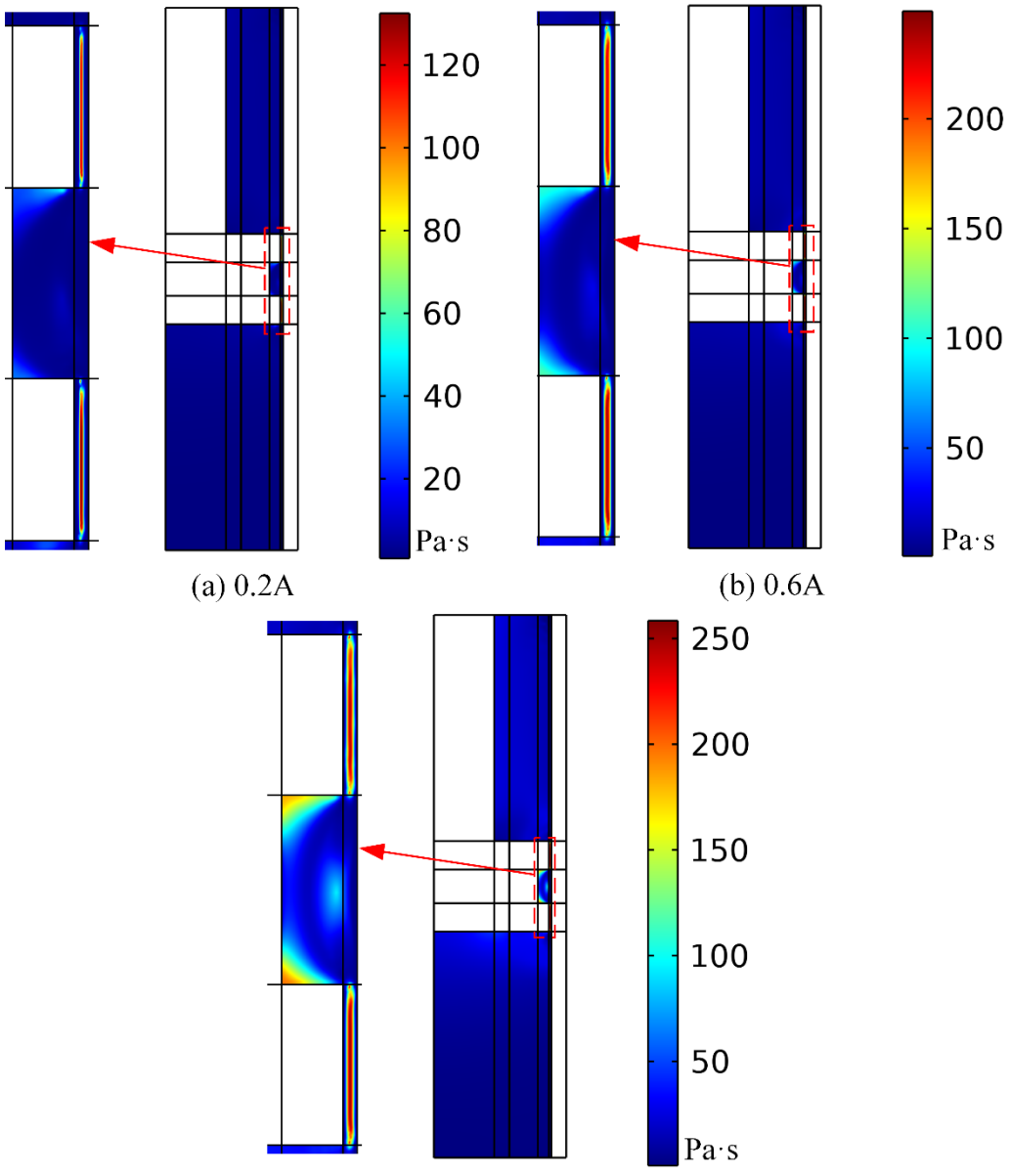

(a) 0.2A (b) 0.6A

(c) 1.4A

Figure 14. The distribution nephogram of the dynamic viscosity

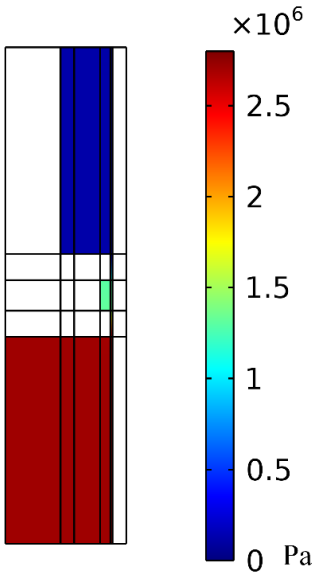

Figure 15. Pressure nephogram with current of 1.4A

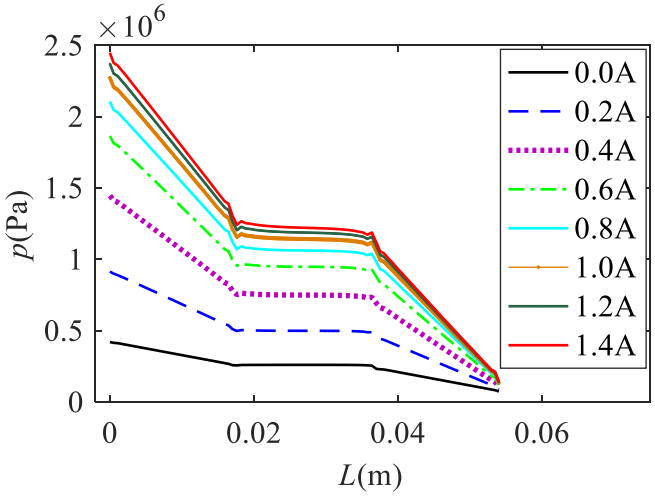

Figure 16. Pressure distribution along the observation path

When the working current of the electromagnetic coil is 1.4A, the internal pressure distribution of the damping structure is shown in Figure 15. It can be seen from Figure 15 that the pressure distribution of the upper and lower chambers is relatively uniform, and there is a large pressure difference between the two chambers. It indicates that the MR hydro-pneumatic spring can produce a large damping force. The pressure distribution curve along the observation path is shown in Figure 16 when the electromagnetic coil is connected with different working currents. It can be seen from Figure 16 that the pressure difference at both ends of the damping channel increases with the increase of current. It indicates that the output damping force of MR hydro-pneumatic spring increases with the increase of current. It can also be seen that the growth trend of the pressure difference with the current slows down when the current reaches 1A. It indicates that the magnetic flux density in the damping channel slows down with the current growth, and the designed magnetic circuit is close to the saturation state. The increase of differential pressure shows the same change law as the magnetic induction intensity.

The total reaction force of MR fluid on the piston is the output damping force of MR hydro-pneumatic spring. Under the sinusoidal excitation with amplitude of 20 mm and frequency of 1 Hz, the relationship curve between the damping force and displacement of the hydro-pneumatic spring under different currents is shown in Figure 17. It can be seen from Figure 17 that the force-displacement curve is symmetrically distributed about the relative equilibrium position. Comparing the damping force-displacement curves under various currents, it can be found that the output damping force of the damper will increase with the increase of the current. It indicates that the magnetic flux density in the damping channel will increase with the increase of the current. The dynamic viscosity of MR fluid increases, which makes the output damping force of the damper increases. When the current reaches a certain value, the damping force no longer increases significantly. It indicates that the internal magnetic circuit of the damper reaches saturation at this time. It can be seen from the figure that the maximum output force of the hydro-pneumatic spring is about 22kN. And the dynamic adjustable multiple is about 6 times. It indicates that the designed MR hydro-pneumatic spring meets the design index and has good damping adjustable characteristics.

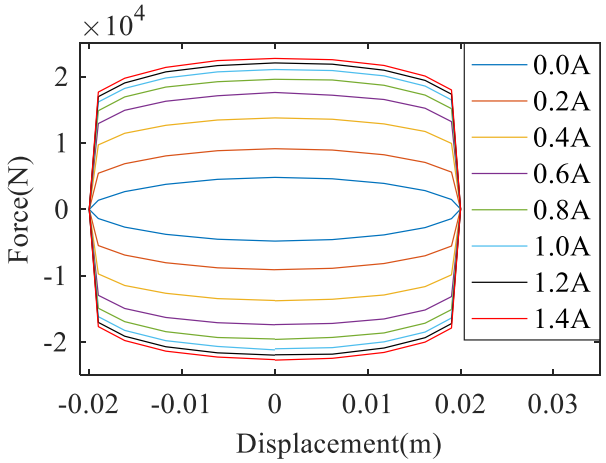

Figure 17. The force-displacement curve

(3) Thermal-flow field simulation results

Combined with electromagnetic field analysis model and thermal-flow analysis model, the thermal-flow analysis of the designed MR damping structure is carried out. The influence of temperature on the density and magnetic field strength of MR fluid is not considered in this analysis process. Under the sinusoidal excitation with the amplitude of 20mm and the frequency of 1Hz, the isotherm line after 10 cycles is shown in Figure 18. It can be seen from Figure 18 that the heat dissipation is mainly concentrated in the relative motion area of the piston and the cylinder under different working currents of the electromagnetic coil. And the heat is mainly transmitted to the piston and the cylinder through the MR fluid. It indicates that the MR fluid produces Poiseuille pressure flow and Couette viscous flow to convert the vibration energy into heat energy for dissipation when the damper moves. It conforms to the action principle of vibration reduction and energy consumption of the MR damper. It can also be seen from Figure 18 that with the increase of current, the temperature of the moving area increases. The damping coefficient of the MR hydro-pneumatic spring increases with

the increase of current, and it has good working performance of consuming vibration energy.

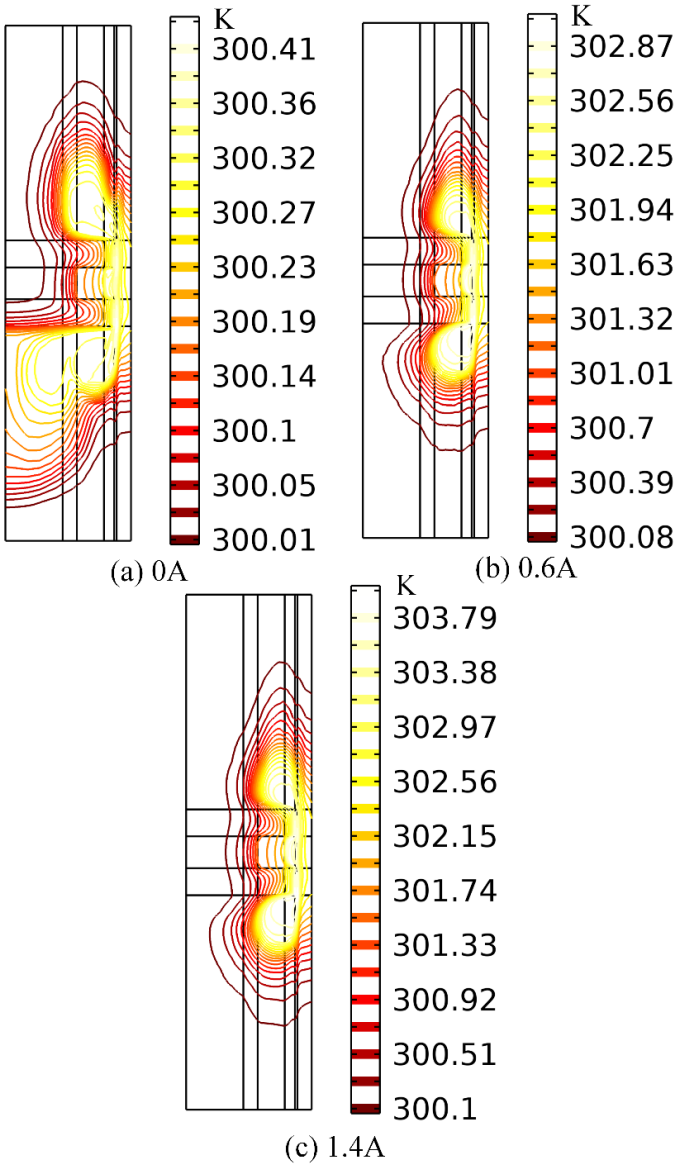

Figure 18. The isotherm line

5. Mechanical properties test and nonlinear modeling of MR hydro-pneumatic spring

5.1 Mechanical properties test

The principle prototype is developed according to the vibration damping structural parameters of the MR hydro-pneumatic spring. The principle prototype is shown in Figure 19 and Figure 20.

Figure 19. The prototype of the MR hydro-pneumatic spring damping structure

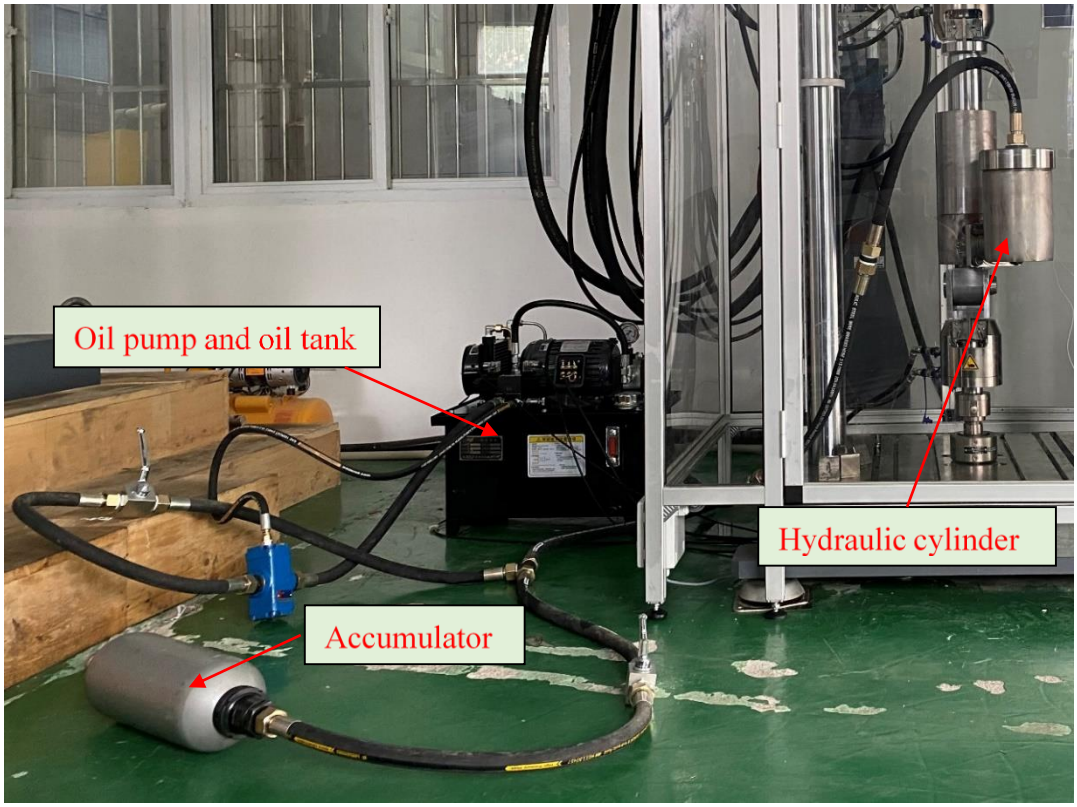

Figure 20. The prototype of the MR hydro-pneumatic spring

The mechanical properties of the MR hydro-pneumatic spring were tested by an electro-hydraulic servo fatigue machine (150kN). The MR hydro-pneumatic spring is mainly used in a heavy armored vehicle. The wheel load of about 5.5t, so the accumulator with a pre-filled pressure of 8Mpa and a volume of 4L is selected in the mechanical properties test. The mechanical properties test system of the MR hydro-pneumatic spring is shown in Figure 21.

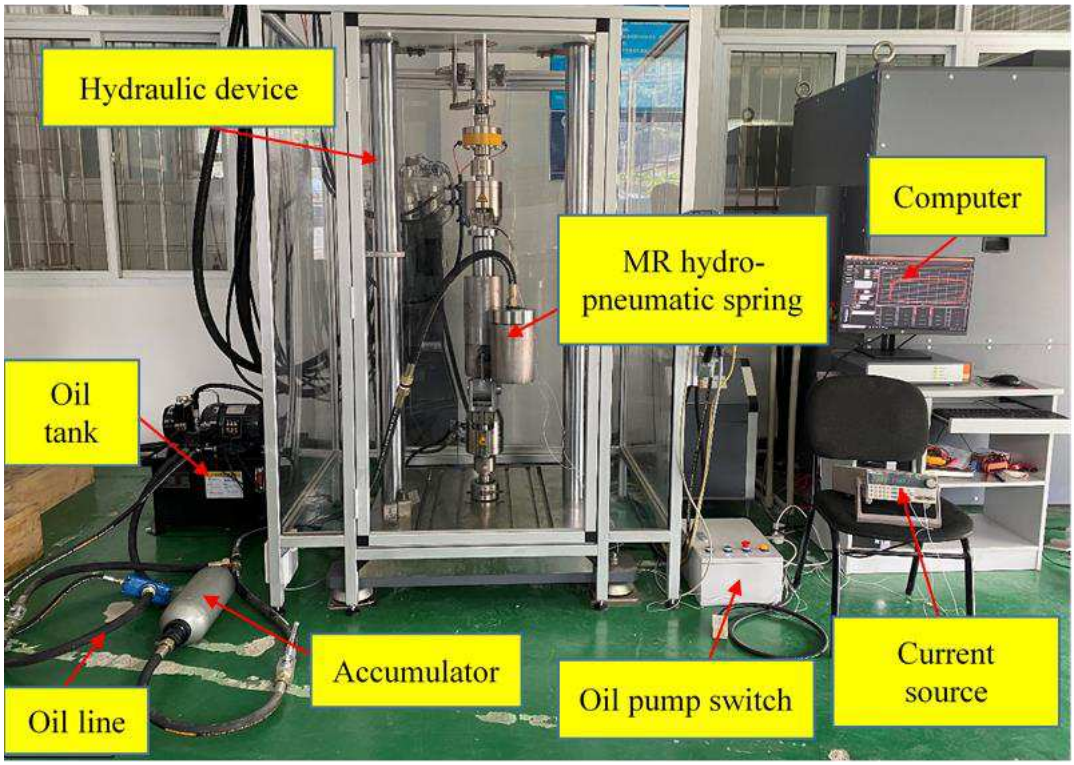

Figure 21. The mechanical properties test system of the MR hydro-pneumatic spring

A sinusoidal signal with an amplitude of 20 mm and a frequency of 1 Hz is used as the excitation. The mechanical properties of MR hydro-pneumatic spring were tested under the working current range of 0~1.4A and the interval of 0.2A. The force-displacement curve and force-velocity curve of the MR hydro-pneumatic spring are obtained through testing, as shown in Figure 22.

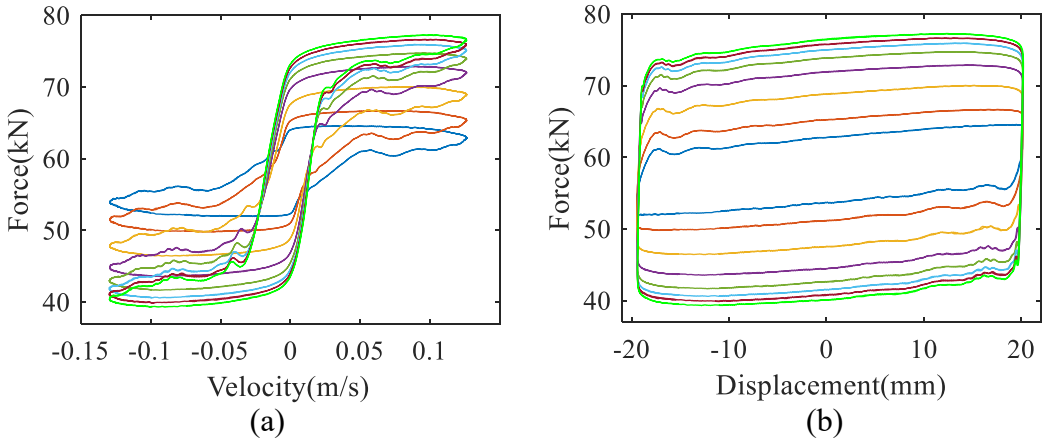

Figure 22. Performance test results of the MR hydro-pneumatic spring: (a) the force-velocity; (b) the damping force-displacement.

It can be seen from Figure 22 that the output force of the MR hydro-pneumatic spring changes up and down in the foundation force. The foundation force is generated by the accumulator. The foundation force is about 57kN. Waves appear in test curves, which is caused by the sudden change of oil flow direction in the oil pipe, friction, residual air and other factors during the test. It can be seen from Figure 22 (a) that there is obvious hysteresis in the force-velocity curve, and the area of hysteresis loop

increases with the increase of current. There are also two distinct regions in the force-velocity curve, namely, the pre yield region and the post yield region. The hysteretic trend of the post yield region increases with the increase of displacement. The area enclosed by the force-velocity curve represents the power of vibration energy consumed by the MR hydro-pneumatic spring, which increases with the increase of current and displacement. It can be seen from Figure 22 (b) that there is an obvious inclination in the force-displacement curve, which is caused by the stiffness of the MR hydro-pneumatic spring. The area enclosed by the force-displacement curve represents the vibration energy consumed by the damper, and the energy dissipation capacity increases with the increase of current. According to the force-velocity curve and the force-displacement curve, the force amplitude increases with the increase of the working current of the electromagnetic coil. When the current reaches 1.4A, the increasing trend of the damping force slows down, showing saturation phenomenon. This is because the MR fluid in the damping channel reaches the magnetic saturation state, and its shear stress reaches the yield state. Output force range of the MR hydro-pneumatic spring at 0A: 52~64kN. Output force range at 1.4A: 39~77kN. Subtracting the foundation force, the maximum damping force is 20kN, and the dynamic adjustable multiple is about 6.4 times. The test results are similar to the simulation analysis results of multiple-physical fields. It indicates that the designed MR hydro-pneumatic spring has reasonable structure, meet the design requirements, and has good damping adjustable characteristics.

5.2 Elastic force calculation model of MR hydro-pneumatic spring

The elastic force produced by the accumulator is mainly used to support the static load and balance the dynamic load of the vehicle body. Generally, the high-pressure gas is nitrogen in the accumulator. Relevant literature shows that the physical properties of nitrogen are similar to the ideal gas, so its elastic force calculation model can be derived from the calculation model of the ideal gas [27-29].

When the vehicle is in the static equilibrium position, the gas in the accumulator is in the isothermal process, and the gas polytropic index $\gamma=1$. The accumulator pressure can be obtained from the force analysis during the static balance of the vehicle body, as shown in Equation (25).

$$P_1=\frac{m_s g}{A_{\text{rod}}} \tag{25}$$

Where, P_1 is the internal pressure of the accumulator in static equilibrium; m_s is the spring-loaded mass of the hydro-pneumatic spring; A_{rod} is the cross-sectional area of the piston rod.

Therefore, the gas volume in the accumulator in the static equilibrium position is shown in Equation (26).

$$V_1=\frac{P_0V_0}{P_1}=\frac{P_0V_0A_{rod}}{m_s g} \tag{26}$$

Where, P_0 and V_0 are pressure and volume of thepre-filled gas in the accumulator, respectively.

Instantaneous volume of gas in accumulator during reciprocating motion is shown in Equation (27).

$$V_s = V_1 + A_{rod} x_q \tag{27}$$

Where, x_q is the relative displacement between the piston and the cylinder.

In the process of the hydro-pneumatic spring reciprocating motion, the vibration energy is attenuated by transforming kinetic energy into heat energy. In this process, the gas in the accumulator can be assumed to be an adiabatic process, namely, the gas variability index γ=1.4. Thus, the real-time gas pressure in the accumulator is shown in Equation (28).

$$P_s = P_1 (V_1 / V_s)^{\gamma} \tag{28}$$

The accumulator is equipped with a pre-filled airbag with a certain pressure. And the elastic force is generated during the reciprocating motion of the hydro-pneumatic spring. From Equation (25) ~ Equation (28), the calculation expression of the elastic force of the accumulator is shown in Equation (29).

$$F_s = m_s g \left(\frac{P_0 V_0}{P_0 V_0 + m_s g x_q}\right)^{\gamma} \tag{29}$$

5.3 Nonlinear model of the MR hydro-pneumatic spring

Bouc-Wen model is widely used to describe the hysteresis characteristics of MR damper because it can produce a series of different hysteresis curves. The Bouc-Wen model is composed of hysteresis system, spring and viscous damping in parallel, as shown in Figure 23. The mathematical expression is shown in Equations (30) and Equation (31) [30].

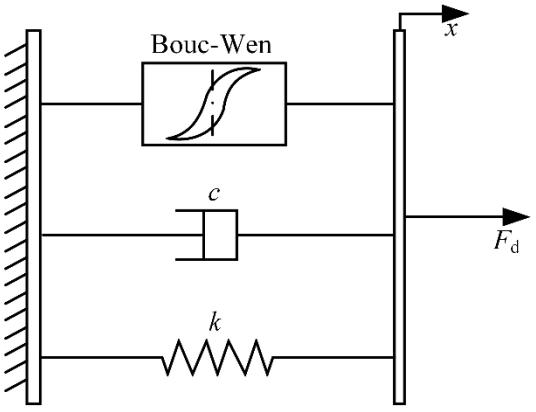

Figure 23. Structural diagram of Bouc–Wen model

$$F_d = c\dot{x} + kx + \alpha\varpi + f_0 \tag{30}$$

$$\dot{\varpi} = \rho[\dot{x} - \sigma|\dot{x}||\varpi|^{n-1}\varpi + (\sigma - 1)|\dot{x}||\varpi|^n] \tag{31}$$

Where, F_{d} is the output force of Bouc–Wen model; x and $\dot{x}$ represent the relative displacements and the relative velocities, respectively; ϖ is the hysteresis operator; c, k and α are viscous coefficient, stiffness coefficient and hysteresis coefficient, respectively; f_0 is the bias force generated by the compensation device during the test; ρ and σ are shape coefficients of hysteresis loops; n is yield slope coefficient.

According to mechanical properties test results of the MR hydro-pneumatic spring, its output force is equal to the sum of the elastic force of the accumulator and the damping force of the MR damper. The force-velocity curve shows obvious hysteretic characteristics. Therefore, the nonlinear model of the MR hydro-pneumatic spring can be established by combining the elastic force calculation model of the accumulator and the Bouc-Wen model of the MR damper. The mathematical expression of Bouc-Wen model of the MR hydro-pneumatic spring can be obtained from Equations (29) to (31), as shown in Equation (32) and Equation (33).

$$F_{d\mathrm{q}} = c\dot{x}_{\mathrm{q}} + \alpha\varpi + F_{\mathrm{s}} \tag{32}$$

$$\dot{\varpi} = \rho[\dot{x}_{\mathrm{q}} - \sigma\left|\dot{x}_{\mathrm{q}}\right|\left|\varpi\right|^{n-1}\varpi + (\sigma-1)\left|\dot{x}_{\mathrm{q}}\right|\left|\varpi\right|^{n}] \tag{33}$$

Where, $F_{d\mathrm{q}}$ is the output force of the MR hydro-pneumatic spring; $\dot{x}_{\mathrm{q}}$ is the relative speed between the piston and the cylinder.

The pre-filled gas pressure of the accumulator is 8Mpa, and the pre-filled gas volume is 4L. Based on the test results of the MR hydro-pneumatic spring under 20mm1Hz sinusoidal excitation, the elastic force calculation model is shown in Equation (34).

$$F_{\mathrm{s}}=58.1\left(\frac{32}{32-58.1x_{\mathrm{q}}}\right)^{1.4} \quad \text{(kN)} \tag{34}$$

Based on my previous research [31, 32], the parameter identification method of MR damper Bouc-Wen model is used to identify the parameters of the MR hydro-pneumatic spring's Bouc-Wen model. The identification results are shown in Table 4.According to Table 4, the relationship between parameters and current is fitted by the least square method. The fitting result is shown in Figure 24, and the mathematical expression is shown in Equations (35) to (37).

Table 4. Identification results of model parameters of MR hydro-pneumatic spring

I(A)	c(kN·s/m)	α(kN)	ρ(m^{-1})	σ	n
0	10.52	3.21	3551	1.5	2
0.2	18.12	5.31	3711	1.5	2
0.4	23.65	7.82	3836	1.5	2
0.6	27.01	10.21	3933	1.5	2
0.8	28.32	12.15	4022	1.5	2
1.0	29.53	13.23	4111	1.5	2
1.2	31.01	13.86	4232	1.5	2
1.4	32.32	14.11	4421	1.5	2

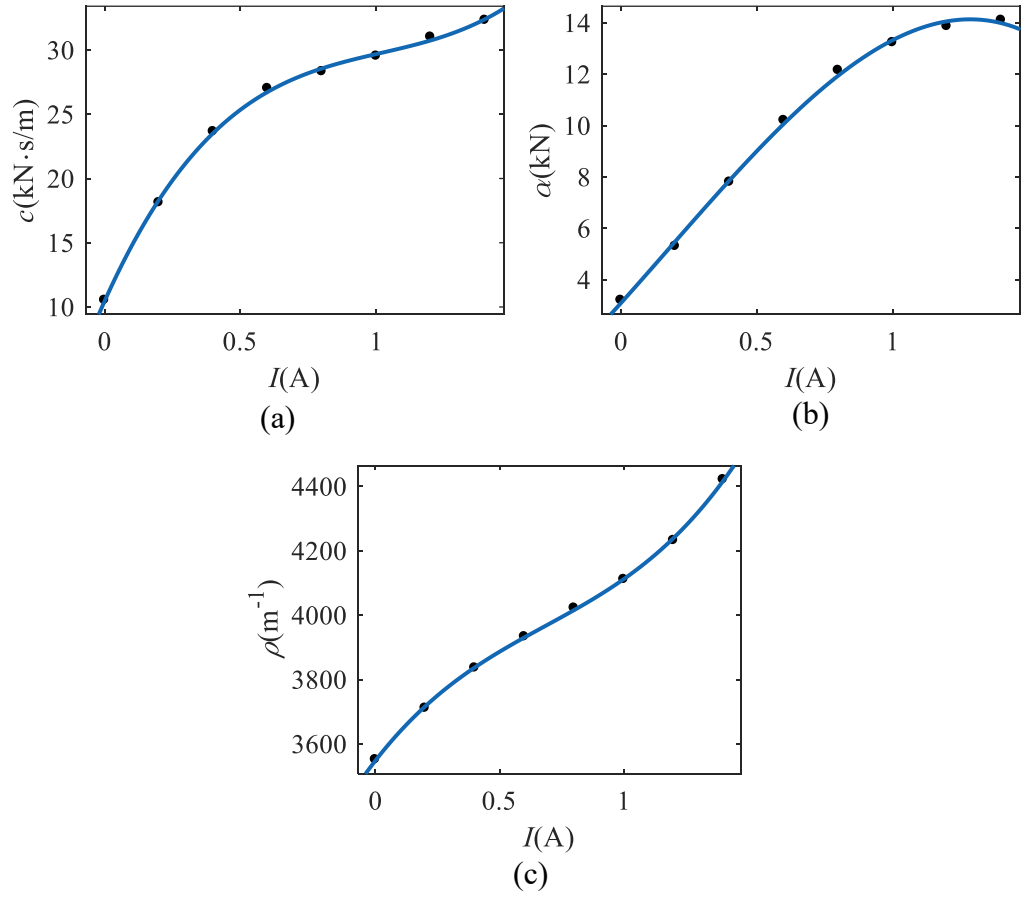

Figure 24. Bouc–Wen model parameters and current fitting curve: (a) the *c*-*I* curve; (b) *α*-*I* curve; (c) *ρ*-*I* curve

$$c = 13.58I^3 - 41.52I^2 + 47.16I + 10.45 \tag{35}$$

$$\alpha = -3.27I^3 + 1.722I^2 + 11.78I + 3.091 \tag{36}$$

$$\rho = 408.1I^3 - 837.6I^2 + 993.6I + 3548 \tag{37}$$

Replace Equations (35) to (37) into Equations (32) and (33), and conduct numerical simulation under the same input excitation (20mm, 1Hz) as the mechanical properties test. The comparison between the numerical simulation results and the test results is shown in Figure 25. The numerical results show that the calculated curve of the established Bouc-Wen model has a high degree of coincidence with the test curve. It indicates that the established Bouc-Wen model of the MR-hydro pneumatic spring can effectively simulate its mechanical behavior.

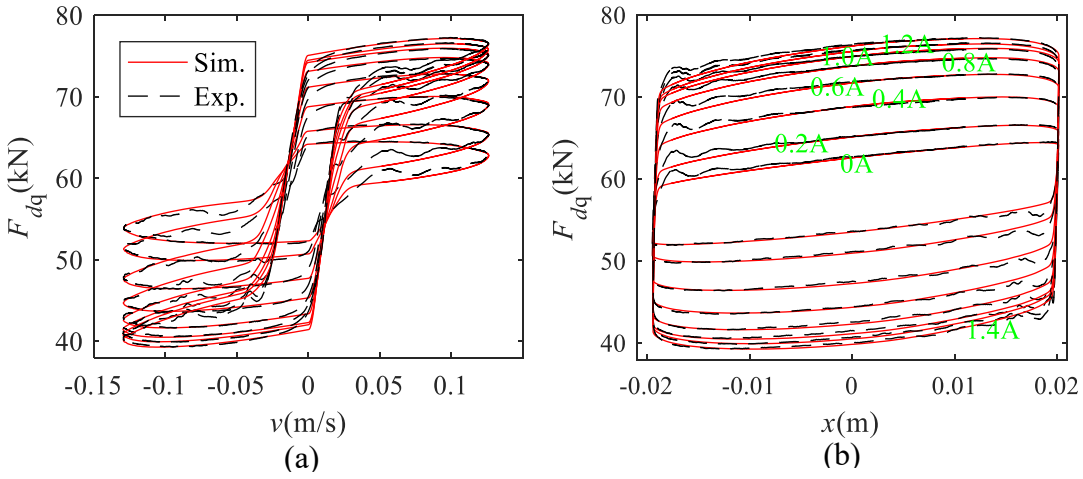

Figure 25. The Bouc–Wen model simulation results of the MR-hydro pneumatic spring: (a) the force–velocity curve; (b) the force–displacement curve

6. Conclusion

In this paper, MR technology is introduced into the traditional hydro-pneumatic suspension system, and a new MR hydro-pneumatic suspension system is proposed. The MR damping structure is the core component of the MR-hydro pneumatic spring. In order to make its structure reasonable and its performance meet the design requirements, this paper completes the design and development of the MR-hydro pneumatic spring based on the theory of electric-magnetic-fluid-solid-thermal multi-physical field coupling analysis. The results of simulation analysis and mechanical properties test show that the designed MR hydro-pneumatic spring has reasonable structure, excellent working performance and meets the design requirements. Based on the test results of mechanical properties, a dynamic model that can accurately describe the nonlinear characteristics of the MR hydro-pneumatic spring is established. It provides a theoretical basis for the subsequent research on the control strategy of the MR hydro-pneumatic suspension. The research done in this paper can provide a theoretical basis for the follow-up research and application of MR hydro-pneumatic suspension system. It can also provide design ideas and analysis methods for relevant magnetorheological damping mechanisms. The main work and conclusions are as follows:

(1) According to the working principle of the traditional hydro-pneumatic suspension system with single air chamber, the MR damping technology is introduced into the hydro-pneumatic suspension, and a new type of shear-valve mode MR hydro-pneumatic spring is proposed.

(2) According to the design requirements, based on the design method of MR damper, the main parameters of MR hydro-pneumatic spring damping structure is designed. The maximum design damping force can reach 16.138kN, the dynamic adjustable multiple is about 7.5. The controllable performance is excellent, which meets the design requirements

(3) The working state and performance of MR hydro-pneumatic spring are affected

by multiple-physical fields at the same time. In order to accurately explore the overall performance of the MR hydro-pneumatic spring under the action of multiple-physical fields, verify the rationality of structure and the process of energy dissipation, the dynamic performance of the designed MR hydro-pneumatic spring is analyzed by using the finite element software Comsol based on the theory of electromagnetic field analysis, flow field analysis and thermal field analysis. The simulation results show that the magnetic circuit structure is reasonable, the internal fluid flow state and heat dissipation process conform to the actual situation. The maximum damping force is about 22kN, and the dynamic adjustable multiple is about 6 times, which meets the design requirements.

(4) The mechanical properties of the MR hydro-pneumatic spring were tested. Under the same excitation conditions, the mechanical properties test results were similar to the simulation results of multiple-physical fields, with a maximum damping force of about 20KN and a dynamic adjustable multiple of about 6.4 times. This shows that the designed MR hydro-pneumatic spring has reasonable structure and good controllable performance. In order to analyze the nonlinear characteristics of the MR hydro-pneumatic spring, a nonlinear model of the MR hydro-pneumatic spring is established by combining the elastic force calculation model of gas with the Bouc-Wen model of MR damper. The numerical simulation results are in good agreement with the experimental results, which shows that the established nonlinear model can accurately describe its dynamic characteristics.

Acknowledgment

This work has been supported by Jiangsu Funding Program for Excellent Postdoctoral Talent.

Data availability

Data sharing not applicable to this article as no datasets were generated or analyzed during the current study.

Declarations

Conflict of interest

The authors declare that they have no conflict of interest.

Reference

[1] Kucuk, K., Yurt, H.K., Arikan K.B., Mrek, H.: Modelling and optimisation of an 8×8 heavy duty vehicle's hydro-pneumatic suspension system. Int. J. Vehicle Des. 71(1-4), 122-138 (2016)

[2] Ali, D., Frimpong, S.: Artificial intelligence models for predicting the performance of hydro-pneumatic suspension struts in large capacity dump trucks. Nt. J. Ind. Ergonom. 67, 283-295 (2018)

[3] Tian, L.L., Gu, Z.Q., Li, W.P., Liang, X.B., Peng, G.P.: Ride comfort simulation and parameters optimization design of nonlinear hydro-pneumatic suspension system. J. Cent. South Unv (Science and Technology). 42(12), 3715-3721 (2011)
[4] Yi, T., Ma, F., Jin, C., Huang, Y.: A novel coupled hydro-pneumatic energy storage system for hybrid mining trucks. Energy. 143, 704-718 (2018)
[5] Yang, B., Chen, S.Z., Wu, Z.C., Yang, L., Zhang, B: Development of a Twin-Accumulator Hydro-Pneumatic Suspension. Journal of Shanghai Jiaotong University(Science). 15(2), 183-187 (2010)
[6] Lin, D.Z., Yang, F., Gong, D., Zhao, F., Luo, X.Y., Li, R.H.: Experimental investigation of two types interconnected hydro-pneumatic struts. IEEE Access. 7, 100626-100637 (2019)
[7] Kamio, S.: The method with the funds strategy of small and medium-sized enterprises : The analysis based on the actual condition. Math Method Appl. Sci. 36, 64-70 (2013)
[8] Giliomee, C.L., Els, P.S.: Semi-active hydropneumatic spring and damper system. J. Terramechanics. 35, 109-117 (1998)
[9] Saglam, F., Unlusoy, Y.S.: Adaptive ride comfort and attitude control of vehicles equipped with active hydro-pneumatic suspension. Int. J. Vehicle Des. 71(1-4), 31-51 (2016)
[10] Yao, G.Z., Yap, F.F., Chen, G., Li, W.H., Yeo, S.H.: MR damper and its application for semi-active control of vehicle suspension system. Mechatronics. 12, 963-973 (2002)
[11] Yildiz, A.S., Sivrioglu, S., Zergeroglu, E., Cetin, S.: Nonlinear adaptive control of semi-active MR damper suspension with uncertainties in model parameters. Nonlinear Dynamics. 79(4), 2753-2766 (2015)
[12] Bai, X.X., Hu, W., Wereley, N.M.: Magnetorheological damper utilizing an inner bypass for ground vehicle suspensions. IEEE T. Magn. 49(7), 3422-3425 (2013)
[13] Parlak, Z., Engin, T., All, S.: Optimal design of MR damper via finite element analyses of fluid dynamic and magnetic field. Mechatronics. 22, 890-903. (2012)
[14] Goldasz, J., Sapinski, B.: Application of CFD to modeling of squeeze mode magnetorheological dampers. Acta Mech. Automatica. 9(3), 129-134 (2015)
[15] Elsaady, W., Oyadiji, S.O., Nasser, A.: A one-way coupled numerical magnetic field and CFD simulation of viscoplastic compressible fluids in MR dampers. Int. J. Mech. Sci. 167, 105265 (2019)
[16] Versaci, M., Cutrupi, A., Palumbo, A.: A magneto-thermo-static study of a magneto-Rheological fluid damper: a finite element analysis. IEEE T. Magn. 57(1), 4600210 (2021)
[17] Chai, Y., Gao, W., Ankay, B., Li, F., Zhang, C.: Aeroelastic analysis and flutter control of wings and panels:A review. IJMSD. 1(1), 5-34 (2021)
[18] Xu, Z., Hao, Z., Xu, W., Mao J.: A full-spectrum analysis of high-speed train interior noise under multi-physical-field coupling excitations. Mech. Syst. Signal Pr. 75, 525-543 (2016)
[19] Jiang, M., Rui, X.T., Yang, F.F., Zhu, W., Zhang, Y.N.: Multi-objective optimization design for a magnetorheological damper. J. Intel. Mat. Syst. Str. 33(1), 33-45 (2022)
[20] Deng, Y.J., Optimal design and dynamic performance research of MR damper based on multi-field coupling model. Master Thesis, Nanchang (2020)
[21] Mazur, P., Nijboer, B.: On the statistical mechanics of matter in an electromagnetic field. I. Derivation of the maxwell equations from electron theory. Physica. 19(1), 971-986 (1953)
[22] Constantin, P., F., C.: Navier-Stokes Equations. University of Chicago Press, Chicago (2020)

[23] Xie, Z.M., Karimi, M., Girimaji, S.S.: Small perturbation evolution in compressible Poiseuille flow: pressure-velocity interactions and obliqueness effects. J. Fluid Mech. 814, 249-276 (2017)
[24] Aydin, O., Avci, M.: Laminar forced convection with viscous dissipation in a Couette-Poiseuille flow between parallel plates. Appl. Energy. 83(8), 856-867 (2006)
[25] Davidzon, M.I.: Newton's law of cooling and its interpretation. Int. J. Heat Mass Tran. 55, 5397-5402 (2012)
[26] Nordstrom, J., Berg, J.: Conjugate heat transfer for the unsteady compressible Navier–Stokes equations using a multi-block coupling. Comput. Fluids. 72, 20-29 (2013)
[27] Wang, Z., Shen, Y., Yang, J.: Mathematical model and characteristics analysis of interconnected hydro-pneumatic suspension. Transactions of the Chinese Society of Agricultural Engineering, 28(5), 60-65 (2012)
[28] Cao, D., Rakheja, S., Su, C.Y.: Dynamic analyses of roll plane interconnected hydro-pneumatic suspension systems. Int. J. Vehicle Des. 47, 51-80 (2008)
[29] Lin, D.Z., Yang, F., Gong, D., Rakheja S.: Design and experimental modeling of a compact hydro-pneumatic suspension strut. Nonlinear Dynam. 100(4), 3307-3320 (2020)
[30] Ikhouane, F., Rodellar, J.: Systems with hysteresis: analysis, identification and control using the Bouc-Wen model. John Wiley & Sons, Hoboken (2007)
[31] Jiang, M., Rui, X.T., Zhu, W., Yang, FF. Zhu, H.T., Jiang, R.L.: Parameter sensitivity analysis and optimum model of the magnetorheological damper's Bouc–Wen model. J. Vib. Control. 27(19-20), 2291-2302 (2021)
[32] Jiang, M., Rui, X.T., Zhu, W., Yang, F.F., Zhang, J.S: Modeling and control of magnetorheological 6-DOF stewart platform based on multibody systems transfer matrix method. Smart Mater. Struct. 29(3), 035029 (2020)